ELSEVIER

Journal of Quantitative Spectroscopy & Radiative Transfer 107 (2007) 1–16

Journal of Quantitative Spectroscopy & Radiative Transfer

www.elsevier.com/locate/jqsrt

Discontinuous spectral element method for solving radiative heat transfer in multidimensional semitransparent media

J.M. Zhao, L.H. Liu*

School of Energy Science and Engineering, Harbin Institute of Technology, 92 West Dazhi Street, Harbin 150001, People's Republic of China

Received 16 December 2006; received in revised form 29 January 2007; accepted 4 February 2007

Abstract

A discontinuous spectral element method (DSEM) is presented to solve radiative heat transfer in multidimensional semitransparent media. This method is based on the general discontinuous Galerkin formulation. Chebyshev polynomial is used to build basis function on each element and both structured and unstructured elements are considered. The DSEM has properties such as *hp*-convergence, local conservation and its solutions are allowed to be discontinuous across interelement boundaries. The influences of different schemes for treatment of the interelement numerical flux on the performance of the DSEM are compared. The *p*-convergence characteristics of the DSEM are studied. Four various test problems are taken as examples to verify the performance of the DSEM, especially the performance to solve the problems with discontinuity in the angular distribution of radiative intensity. The predicted results by the DSEM agree well with the benchmark solutions. Numerical results show that the *p*-convergence rate of the DSEM follows exponential law, and the DSEM is stable, accurate and effective to solve multidimensional radiative transfer in semitransparent media.

Keywords: Discontinuous Galerkin method; Spectral element method; Radiative heat transfer; Ray effect

1. Introduction

Numerical methods for solving radiative transfer can be classified into two types, one is the method based on the discretization of radiative transfer equation, and the other is the method based on ray-tracing technique. In recent years, the method based on the discretization of radiative transfer equation, such as discrete ordinate method (DOM) [1], finite-volume method (FVM) [2–4], and finite-element method (FEM) [5,6], have received considerable attention for their advantages such as being flexible to deal with complex media and boundary property, easy and efficient to treat multidimensional problems as compared to the ray-tracing-based methods, such as Monte Carlo method [7] and zonal method [8].

Recently, the discontinuous Galerkin (DG) method was introduced to the solution of radiative transfer problems. Cui and Li [9,10] presented a DG FEM for solving the radiative transfer in emitting, absorbing, and scattering media, in which the linear approximation was used on each element. Liu et al. [11] applied the DG

*Corresponding author. Tel.: +86 451 86402237; fax: +86 451 86221048.
E-mail address: lhliu@hit.edu.cn (L.H. Liu).

0022-4073/$ - see front matter © 2007 Elsevier Ltd. All rights reserved.
doi:10.1016/j.jqsrt.2007.02.001

Nomenclature

$\mathbf{H}$	matrix defined in Eqs. (14b) and (15b)
I	radiative intensity, W/(m^{2}sr)
I_b	black body radiative intensity, W/(m^{2}sr)
K	the kth element
K_{tr}	triangular element
K_{st}	standard element
M	number of discrete ordinate direction
$\mathbf{M}$	matrix defined in Eqs. (14a) and (15a)
$\mathbf{n}$	unit outward normal vector
$\mathbf{n}_{\partial K}$	unit outward normal vector of the boundary of element K
N_{el}	total number of elements
N_{sol}	total number of solution nodes
p	order of polynomial expansion
q	radiative heat flux, W/m^2
$\mathbf{r}$	spatial coordinates vector
S	source term function defined by Eq. (2)
T	temperature, K
w	weight of discrete ordinates approximation
W	weight function
x, y, z	cartesian coordinates
β	extinction coefficient $\beta = (\kappa + \sigma_S)$, m^{-1}
ε_w	wall emissivity
ϕ	nodal basis function
Φ	scattering phase function
μ, η, ξ	direction cosine of radiation direction
κ	absorption coefficient, m^{-1}
σ_S	scattering coefficient, m^{-1}
σ	Stefan-Boltzmann constant, W/(m^{2}K^4)
τ_L	optical thickness, $\tau_L = \beta L$
ω	single scattering albedo
$\mathbf{\Omega}$, $\mathbf{\Omega}'$	unit vector of radiation direction
Ω	solid angle
ζ, γ, ς	cartesian coordinates defined in standard element

Subscripts

i, j	spatial node index
w	value at wall

Superscripts

m, m'	the mth discrete ordinate direction

FEM to solve radiative transfer in graded index media. All of these works initially demonstrated that the DG approach is a very promising method for the solution of radiative transfer problems in both regular and irregular geometries using either structured or unstructured meshes. The DG method has many advantages comparing to the conventional Galerkin method and has been successfully applied to the solution of many physics and engineering problems [12–15]. In DG method, the inter-element continuity is released and the

approximation space composes of discontinuous functions. The DG method is considered to combine both the advantages of FVM and FEM. The main virtues of the DG method can be summarized as: (1) it is element-wise conservative and stable, (2) high-order accurate and polynomials of arbitrary degree can be employed at each element, which make the DG method ideal to be used with *hp*-adaptive strategies, (3) the method can be defined on very general meshes, including non-conforming meshes and (4) it is easy to be implemented and solved element by element. Introduction and comprehensive review of the DG method are referred to Cockburn et al. [16,17].

Spectral-element method (SEM) was originally proposed by Patera [18] for the solution of fluid flow problem. In the SEM, the physical domain is broken up into several elements and within each element a spectral representation based on orthogonal polynomials (such as Chebyshev polynomial and Legendre polynomial) is used. SEM combines the competitive advantages of high-order spectral method, i.e. the *p*-convergence property, and FEM, i.e. the flexibility to deal with complex domain and offering *h*-convergence property. SEM has been successfully applied in computational fluid dynamics and heat transfer [18–21]. Recently, by considering that the equation of radiative transfer (RTE) is in a form of convection-dominated equation [22] and the convection term may cause non-physical oscillation of the solutions of standard Galerkin scheme-based methods, Zhao and Liu [23,24] developed a least-square SEM (LSSEM) for solving multidimensional radiative transfer problems in uniform and graded index media, in which the least-square scheme instead of the standard Galerkin scheme of SEM (GSEM) is used to enhance the stability of the method to solve the RTE. These works demonstrated that higher-order spectral approximation on each element is effective to solve multidimensional radiative transfer problems. However, both the GSEM and the LSSEM are based on global continuous formulation, in which the functions of approximation space are not allowed to be discontinuous across elements, thus lack the salient properties of the method based on the DG formulation described above.

To combine both the advantages of the SEM and the DG method, in this paper, based on the general DG formulation, we present a discontinuous SEM (DSEM) to solve radiative heat transfer in multidimensional semitransparent media, in which Chebyshev polynomial is used to build basis function on each element. The influences of different schemes for the treatment of interelement numerical flux are compared and the *p*-convergence characteristics of the DSEM are studied. The performance of the DSEM is verified by various test examples on meshes with both structured and unstructured elements.

2. Mathematical formulation

2.1. Discrete-ordinates equation of radiative transfer

The discrete-ordinates equation of radiative transfer in the enclosure filled with absorbing, emitting, and scattering gray media can be written in Cartesian coordinates as

$$\nabla \bullet [\mathbf{\Omega}^m I^m(\mathbf{r})] + \beta I^m(\mathbf{r}) = S^m(\mathbf{r}), \tag{1}$$

where the source term $S^m(\mathbf{r})$ is defined as

$$S^m(\mathbf{r}) = \kappa I_b(\mathbf{r}) + \frac{\sigma_S}{4\pi} \sum_{m'=1}^{M} I^{m'}(\mathbf{r}) \Phi(\mathbf{\Omega}^m, \mathbf{\Omega}^{m'}) w^{m'}. \tag{2}$$

For the opaque and diffuse boundary, the boundary conditions are given as

$$I_w^m = \varepsilon_w I_{bw} + \frac{1-\varepsilon_w}{\pi} \sum_{\mathbf{n}_w \bullet \mathbf{\Omega}^{m'} > 0} I_w^{m'} \left| \mathbf{n}_w \bullet \mathbf{\Omega}^{m'} \right| w^{m'}, \quad \mathbf{\Omega}^m \bullet \mathbf{n}_w < 0, \tag{3}$$

where $\mathbf{\Omega}^m$ is the discrete direction vector, $\beta = (\kappa + \sigma_S)$ is the extinction coefficient, κ and σ_S are the absorption and scattering coefficients, respectively, Φ is the scattering phase function, ε_w is the wall emissivity and $w^{m'}$ is the weight of direction $\mathbf{\Omega}^{m'}$ for angular quadrature.

The partial differential Eq. (1) with boundary condition given by Eq. (3) is solved for each discrete direction. The discrete ordinates equation Eq. (1) is in a form as a convection-dominated equation [22]. The convection

term may cause non-physical oscillatory of solutions. This type of instability can occur in many numerical methods including finite difference method and FEM if no special stability treatment is taken. In Section 2.2, a DSEM was developed to solve the discrete-ordinates equation of radiative heat transfer.

2.2. General DG formulation

Unlike the continuous Galerkin solution scheme, which uses global basis function and weight function, the DG scheme uses basis and weight function locally defined on each element. In DG solution scheme, the information transfer across element boundaries is imposed by modeling the numerical flux. Details on description and discussion of the features of the DG method are referred to Ref. [16]. For each element K, Eq. (1) is weighted by W and integrated over K using Gauss divergence theorem

$$-<I,\boldsymbol{\Omega}\bullet\nabla W>_K+(\widehat{\boldsymbol{\Omega}I}\bullet\mathbf{n}_{\partial K},W)_{\partial K}+<\beta I,W>_K=<S,W>_K. \tag{4}$$

Without ambiguity the superscript m is omitted, where $\mathbf{n}_{\partial K}$ denotes the unit outward normal vector of the boundary of element K and the operators $<\bullet,\ \bullet>$ and $(\bullet,\ \bullet)$ are defined as

$$<f,g>_K=\int_K fg\,\mathrm{d}V,\quad (f,g)_{\partial K}=\int_{\partial K}fg\,\mathrm{d}A, \tag{5}$$

Here, $\widehat{\boldsymbol{\Omega}I}$ is the numerical flux across element boundaries to be modeled. In this paper, two numerical schemes are considered to model $\widehat{\boldsymbol{\Omega}I}$. The first scheme considered is the classical up-winding scheme, in which the numerical flux is modeled as

$$\widehat{\boldsymbol{\Omega}I}=\boldsymbol{\Omega}\{I\}+\boldsymbol{\Omega}\,\mathrm{sign}(\boldsymbol{\Omega}\bullet\mathbf{n}_{\partial K})[\![\,I\,]\!], \tag{6}$$

where the operator $\{\bullet\}$ and $[\![\,\bullet\,]\!]$ denote the mean value and the jump value of arguments across interelement boundary

$$\{I\}=\frac{1}{2}\left(I^+ + I^-\right),\quad [\![\,I\,]\!]=\frac{1}{2}\left(I^+ - I^-\right). \tag{7}$$

Here the superscript operator "+" and "−" denote the values at the boundary inside element K and outside element K, respectively, which are defined as

$$I^+=\lim_{\delta\to 0}I(\mathbf{r}_{\partial K}-\delta\mathbf{n}_{\partial K}),\quad I^-=\lim_{\delta\to 0}I(\mathbf{r}_{\partial K}+\delta\mathbf{n}_{\partial K}). \tag{8}$$

It can be seen that the numerical flux defined by Eq. (6) is composed of two parts, the mean value part and the jump value part or discontinuity part, and the latter accounts for the discontinuity on the element boundary. Fig. 1 shows the relation between the variables defined on the element K for a good understanding of the description above. By substituting Eq. (6) into Eq. (4) and using the definition given by Eq. (7), the

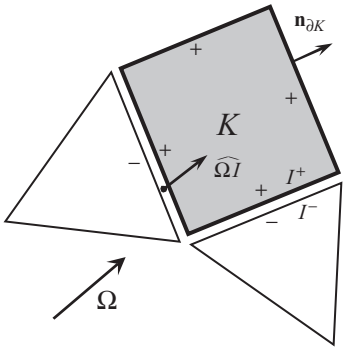

Fig. 1. Schematic diagram of the relations of variables defined in discontinuous Galerkin formulation.

general DG formulation of RTE for up-winding scheme is obtained as

$$-<I,\boldsymbol{\Omega}\bullet\nabla W>_K+\frac{1}{2}\left((\boldsymbol{\Omega}\bullet n_{\partial K}+|\boldsymbol{\Omega}\bullet n_{\partial K}|)I^+,W\right)_{\partial K}+<\beta I,W>_K$$
$$=<S,W>_K-\frac{1}{2}((\boldsymbol{\Omega}\bullet n_{\partial K}-|\boldsymbol{\Omega}\bullet n_{\partial K}|)I^-,W)_{\partial K}. \tag{9}$$

The second scheme considered is the local Lax-Friedrichs scheme. The numerical flux is modeled as

$$\widehat{\boldsymbol{\Omega}I}=\boldsymbol{\Omega}\{I\}+|\boldsymbol{\Omega}|[\![I]\!]\mathbf{n}_{\partial K}. \tag{10}$$

The general DG formulation of RTE for local Lax-Friedrichs scheme is obtained as

$$-<I,\boldsymbol{\Omega}\bullet\nabla W>_K+\frac{1}{2}\left((\boldsymbol{\Omega}\bullet n_{\partial K}+|\boldsymbol{\Omega}|)I^+,W\right)_{\partial K}+<\beta I,W>_K$$
$$=<S,W>_K-\frac{1}{2}((\boldsymbol{\Omega}\bullet n_{\partial K}-|\boldsymbol{\Omega}|)I^-,W)_{\partial K}. \tag{11}$$

It should be noted that the modulus $|\boldsymbol{\Omega}|$ is $|\mu|$, $\sqrt{\mu^2+\eta^2}$ and 1 for one-, two- and three-dimensional problem, respectively. It can be seen that Eqs. (9) and (11) are identical in one-dimensional case.

2.3. Spectral element discretization

Here, the nodal basis functions on each element are constructed by Chebyshev polynomial expansion. The one-dimensional nodal basis functions are Lagrange interpolation polynomials through the Chebyshev–Gauss–Lobatto points. Multidimensional nodal basis functions on structured element (quadrilateral, cube) are constructed by tensor product from one-dimensional nodal basis functions. The construction of nodal basis functions on quadrilateral element was described detailedly in Ref. [23]. For the construction of nodal basis functions on triangular element, if we consider the triangular as a degenerated quadrilateral, namely, with four nodes as shown in Fig. 2, then the same tensor product procedure can be used to build the nodal basis function on the triangular element K_{tr}. But special treatment on the nodal basis of node 1 of the triangular element K_{tr} is still needed. The nodal basis function of node 1 of K_{tr} is selected as the sum of all nodal basis functions mapped from edge 4 (defined by nodes 1 and 4) of the standard quadrilateral element K_{st}.

The unknown radiative intensity is approximated on element K by nodal basis function with Kronecker Delta property as

$$I(\mathbf{r})\simeq\sum_{i=1}^{N_{sk}}I_i\phi_i(\mathbf{r}), \tag{12}$$

where ϕ_i is the nodal basis function defined on K, I_i denotes radiative intensity at solution nodes i and N_{sk} is the number of solution nodes on K. By substituting the approximation of radiative intensity (Eq. (12)) into the DG formulation of RTE (Eq. (9) or Eq. (11)) and taking the weight function W as nodal basis function $\phi_j(\mathbf{r})$, the DSEM discretization of the RTE can be written in matrix form on element K as

$$\mathbf{M}^m\mathbf{I}^m=\mathbf{H}^m, \tag{13}$$

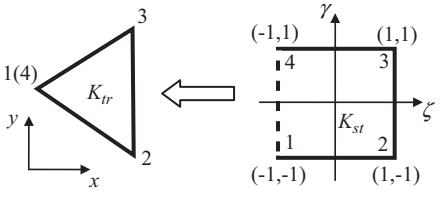

Fig. 2. Schematic diagram of the coordinates transform from stand element to triangular element.

here, the matrices $\mathbf{M}^m$ and $\mathbf{H}^m$ are defined as

$$M_{ji}^m = -<\phi_i, \mathbf{\Omega}^m \bullet \nabla\phi_j>_K + \frac{1}{2}\left((\mathbf{\Omega}^m \bullet \mathbf{n}_{\partial K} + |\mathbf{\Omega}^m \bullet \mathbf{n}_{\partial K}|)\phi_i, \phi_j\right)_{\partial K} <\beta\phi_i, \phi_j>_K, \tag{14a}$$

$$H_j^m = <S^m, \phi_j>_K - \frac{1}{2}\left((\mathbf{\Omega}^m \bullet \mathbf{n}_{\partial K} - |\mathbf{\Omega}^m \bullet \mathbf{n}_{\partial K}|)I^{m,-}, \phi_j\right)_{\partial K}. \tag{14b}$$

For the classical up-winding numerical flux scheme or

$$M_{ji}^m = -<\phi_i, \mathbf{\Omega}^m \bullet \nabla\phi_j>_K + \frac{1}{2}\left((\mathbf{\Omega}^m \bullet \mathbf{n}_{\partial K} + |\mathbf{\Omega}^m|)\phi_i, \phi_j\right)_{\partial K} <\beta\phi_i, \phi_j>_K, \tag{15a}$$

$$H_j^m = <S^m, \phi_j>_K - \frac{1}{2}\left((\mathbf{\Omega}^m \bullet \mathbf{n}_{\partial K} - |\mathbf{\Omega}^m|)I^{m,-}, \phi_j\right)_{\partial K} \tag{15b}$$

for the local Lax-Friedrichs numerical flux scheme.

For the local Lax-Friedrichs numerical flux scheme, the angular ordinates can be completely separated from spatial coordinates, thus a more efficient algorithm can be obtained. The matrices $\mathbf{M}$ defined by Eq. (15a) can be written as

$$M_{ji}^m = -\mathbf{\Omega}^m \bullet <\phi_i, \nabla\phi_j>_K + \frac{1}{2}\mathbf{\Omega}^m \bullet (\mathbf{n}_{\partial K}\phi_i, \phi_j)_{\partial K} + \frac{1}{2}|\mathbf{\Omega}^m|(\phi_i, \phi_j)_{\partial K} <\beta\phi_i, \phi_j>_K \tag{16}$$

with the nodal basis function interpolation technique, namely

$$<f, \phi_j> = \sum_{i=1}^{N_{\text{esol}}} f_i <\phi_i, \phi_j>, \quad (f, \phi_j) = \sum_{i=1}^{N_{\text{esol}}} f_i(\phi_i, \phi_j), \tag{17}$$

then the matrix $\mathbf{H}$ defined by Eq. (15b) can be written as

$$H_j^m = \sum_{i=1}^{N_{\text{esol}}} S_i^m <\phi_i, \phi_j>_K - \frac{1}{2}\mathbf{\Omega}^m \bullet \sum_{i=1}^{N_{esol}} I_i^{m,-}(\mathbf{n}_{\partial K}\phi_i, \phi_j)_{\partial K} + \frac{1}{2}|\mathbf{\Omega}^m| \sum_{i=1}^{N_{\text{esol}}} I_i^{m,-}(\phi_i, \phi_j)_{\partial K}. \tag{18}$$

As a result, all the component matrices of $\mathbf{M}$ and $\mathbf{H}$, namely, $<\phi_i, \nabla\phi_j>_K$, $(\mathbf{n}_{\partial K}\phi_i, \phi_j)_{\partial K}$, $(\phi_i, \phi_j)_{\partial K}$, $<\beta\phi_i, \phi_j>_K$ and $<\phi_i, \phi_j>_K$ only need to be computed once for all discrete ordinates $\mathbf{\Omega}^m$.

2.4. Solution procedures

Because the source term of the discrete-ordinates equation in direction m contains the radiative intensities of the other directions, global iteration similar to those used in the DOM are necessary to update the source term. A spatial loop is needed to solve by the DSEM element by element and a spatial iteration is needed to ensure the radiative intensity of each angular direction is converged. On each element the matrix equations given by Eq. (13) are solved by Gaussian elimination. The implementation of the DSEM can be carried out according to the following routine:

Step 1: Mesh the solution domain.

Step 2: Begin the global iteration.

Step 3: Angular loop. Loop each angular direction $\mathbf{\Omega}^m$.

Step 4: Begin the spatial iteration.

Step 5: Spatial loop. Loop each element K, choose the order of Chebyshev polynomial and generate the solution nodes for each element with Gauss–Chebyshev–Lobatto points.

Step 6: Build the nodal basis function for each element K from standard element K_{st}, and integrate to get the matrix $\mathbf{M}^m$ and $\mathbf{H}^m$ defined in Eq. (14) and Eq. (15).

Step 7: Solve the matrix equation Eq. (13) to get the radiative intensity on element K for direction $\mathbf{\Omega}^m$.

Step 8: If the spatial iteration converged then go to Step 3, otherwise continue the spatial iteration.

Step 9: Terminate the iteration process if the stop criterion is satisfied. Otherwise go back to Step 3.

In this paper, the maximum relative error 10^{-4} of radiative intensity $\left(\|I_{\text{new}} - I_{\text{old}}\|/\|I_{\text{new}}\|\right)$ is taken as the stop criterion for the spatial iteration and the global iteration.

3. Results and discussion

To verify the performance of the DSEM presented in this paper, four various test cases are selected. For the sake of quantitative comparison to the benchmark results, the integration averaged relative error of the DSEM solution is defined as

$$\text{Relative error } \% = \frac{\int|\text{DSEM solution} - \text{Benchmark result}|\,\mathrm{d}x}{\int|\text{Benchmark result}|\,\mathrm{d}x} \times 100. \tag{19}$$

3.1. Case 1: Gaussian-shaped radiative source term between infinite parallel black plates

We consider the radiative transfer between one-dimensional black parallel plates. The radiative source term within the media is a Gaussian-shaped function. This problem is modeled by the RTE as

$$\mu\frac{\mathrm{d}I}{\mathrm{d}x} + \beta I = \mathrm{e}^{-(x-c)^2/\alpha^2}, \quad x, c \in [0,1] \tag{20}$$

with the following boundary conditions:

$$I(0,\mu) = \mathrm{e}^{-c^2/\alpha^2}, \quad \mu > 0, \tag{21a}$$

$$I(0,\mu) = \mathrm{e}^{-(1-c)^2/\alpha^2}, \quad \mu < 0. \tag{21b}$$

The analytical solution of this problem in the case of $\mu > 0$ can be written as

$$I(x,\mu) = I(0,\mu)\exp\left(-\frac{\beta x}{\mu}\right) - \frac{\alpha\sqrt{\pi}}{2\mu}\exp\left\{-\frac{\beta}{\mu}\left[x - \left(\frac{\alpha^2\beta}{4\mu} + c\right)\right]\right\}\left[\mathrm{erf}\left(\frac{\alpha\beta}{2\mu} + \frac{c-x}{\alpha}\right) - \mathrm{erf}\left(\frac{\alpha\beta}{2\mu} + \frac{c}{\alpha}\right)\right]. \tag{22}$$

This case was also studied in Ref. [25] and served as a good case for testing the stability of the solution methods. The DSEM was applied to this case for $c = 0.5$, $\alpha = 0.02$, $\mu = 1.0$ and $\beta = 1.0$. Fig. 3 shows radiative intensities obtained by the DSEM with uniform 20 elements and fourth-order polynomial and compared to the analytical solution. The results obtained by Galerkin SEM (GSEM) [23] with the same spatial grid is also presented as a comparison. It can be seen that the result obtained by the DSEM is accurate and stable, while the result of the GSEM exhibits obvious non-physical oscillations, which was due to the instability of continuous Galerkin formulation for solving convection-dominated problem with large gradient existing in the solution. The p-convergence characteristics of the DSEM are shown in Fig. 4 for three values of extinction

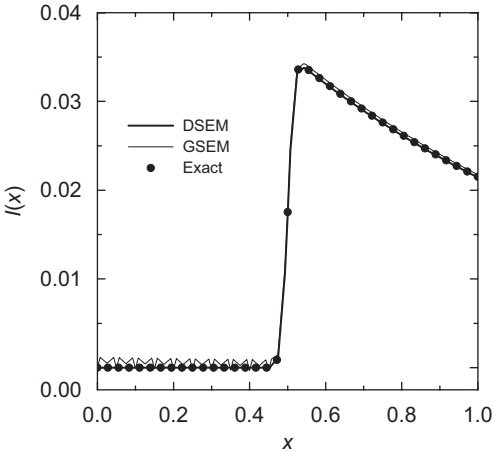

Fig. 3. Radiative intensity distribution between the parallel plates.

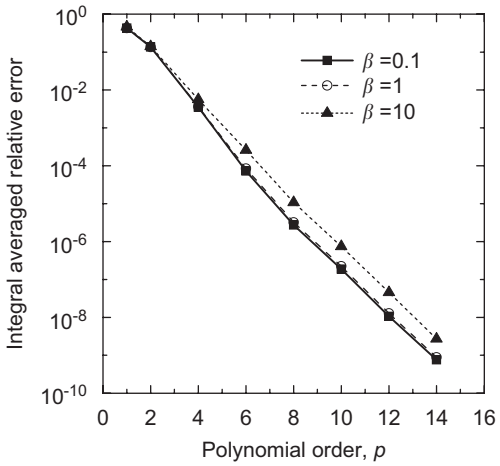

Fig. 4. The p-convergence characteristics of the DSEM for 1D case.

coefficient, namely $\beta = 0.1$, 1 and 10. It can be seen that the p-convergence rates of the DSEM are very fast and follow exponential law for different values of extinction coefficient.

3.2. Case 2: anisotropically scattering in a square enclosure

In this case, we consider radiative heat transfer in a two-dimensional black square enclosure filled with anisotropically scattering media. The optical thickness based on the side length L of the square enclosure is $\tau_L = \beta L = 1.0$. The media temperature T_g is kept as 1000 K, but the temperatures of all boundary walls are maintained at 0 K. This case was also studied by Kim and Lee [26] using the DOM. The scattering phase function of the media is the F2 phase function given by Eq. (23) with asymmetry factor of 0.66972.

$$\mathbf{\Phi} = \sum_{j=0}^{8} C_j P_j(\mu), \tag{23}$$

where the P_j are the Legendre polynomials. The C_j are the expansion coefficients defined as $C_0 = 1.0$, $C_1 = 2.00917$, $C_2 = 1.56339$, $C_3 = 0.67407$, $C_4 = 0.22215$, $C_5 = 0.04725$, $C_6 = 0.00671$, $C_7 = 67407$ and $C_8 = 0.00005$, respectively.

The DSEM was applied to this case for three values of single scattering albedo ω, namely 0.0, 0.5, and 0.9. The S_8 approximation is used for angular discretization. Three spatial decomposition schemes, namely, uniform four quadrilateral elements (Q4), 26 and 62 triangular elements (T26 and T62), with 4th order polynomial are used. The decomposition and spectral node distribution of the T26 scheme is shown in Fig. 5. The dimensionless net radiative heat fluxes on the bottom wall obtained by employing the classical up-winding numerical flux scheme are shown in Fig. 6 for different values of scattering albedo and compared to the results obtained by Kim and Lee using the DOM [26]. It can be seen that, even for the decomposition with four elements (Q4), the DSEM results has a good accuracy. The maximum integral averaged relative error based on the result of the DOM [26] is less than 0.8%. The DSEM approach has good accuracy in solving the radiative heat transfer in anisotropically scattering media.

To verify the performance of different numerical flux modeling schemes used in the DSEM for solving the RTE, Fig. 7 shows a comparison of dimensionless net radiative heat flux on the bottom wall obtained by using the classical up-winding numerical flux scheme and the local Lax-Friedrichs numerical flux scheme for the case of $\omega = 0.5$. As can be seen from Fig. 7, for the coarse decomposition (Q4), the difference of dimensionless net radiative heat flux obtained by using these two numerical flux modeling schemes is more evident on the left and the right bottom corners of the square enclosure, and the former scheme gives better result, while with refining of the decomposition (to T26), the difference of results obtained by using these two numerical flux

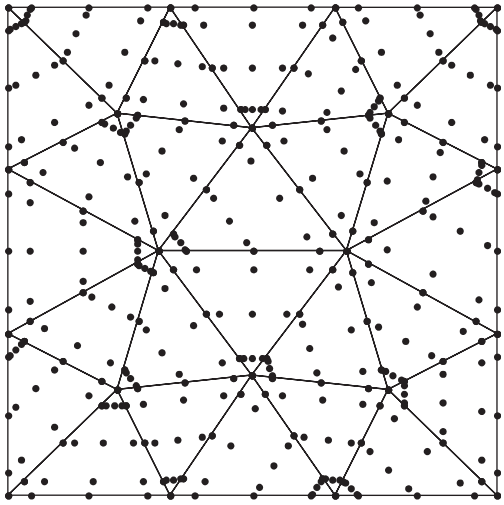

Fig. 5. Solution domain decomposition and spectral nodes distribution (26 elements).

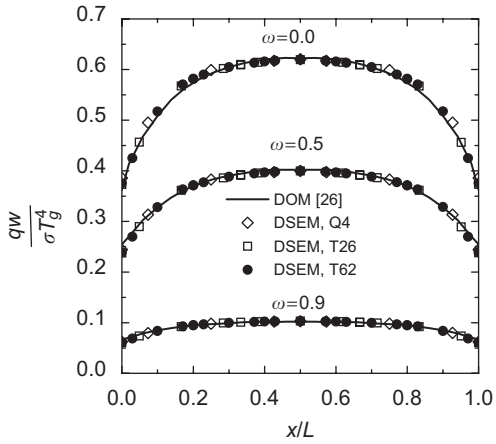

Fig. 6. Dimensionless net radiative heat flux distribution along the bottom wall of square enclosure filled with anisotropically scattering media.

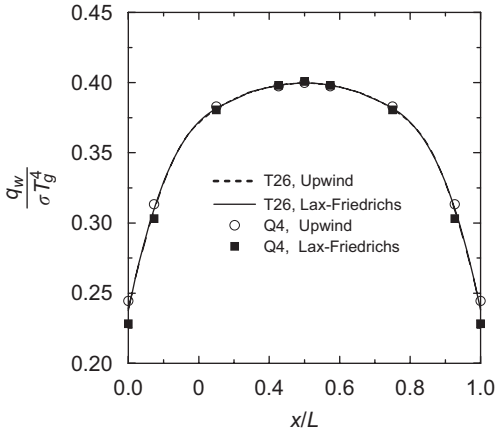

Fig. 7. Comparison of dimensionless net radiative heat flux distribution obtained by DSEM with different schemes of numerical flux.

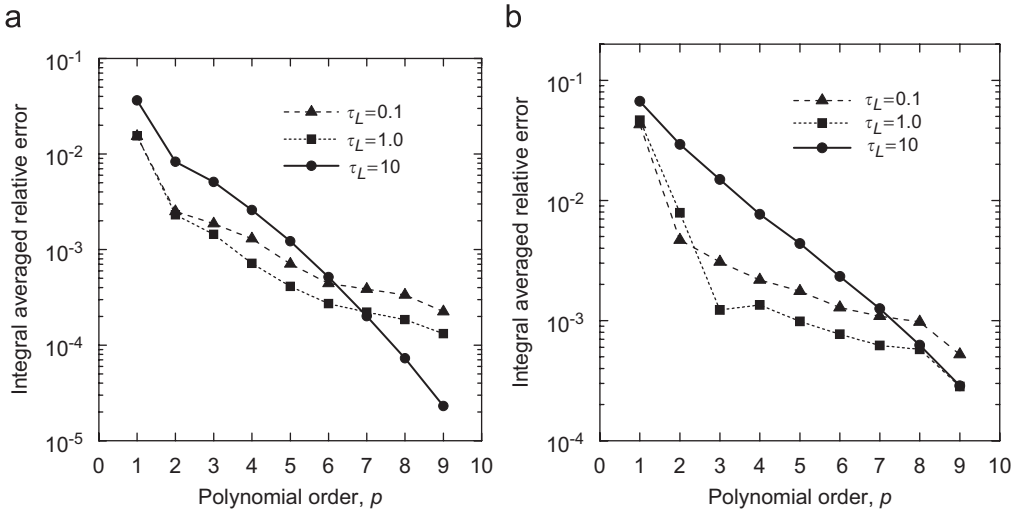

Fig. 8. The *p*-convergence characteristics of the DSEM for solution with (a) quadrilateral elements (Q25) and (b) triangular elements (T26).

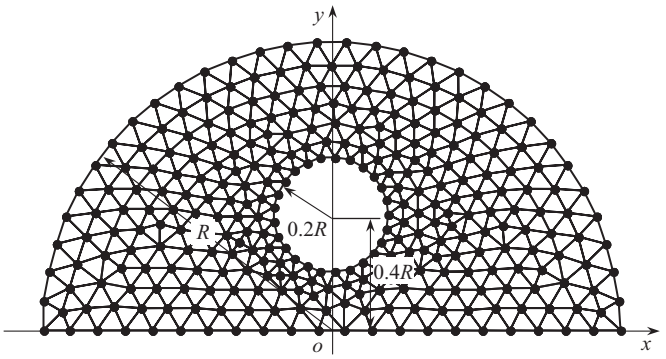

Fig. 9. Solution domain and mesh decomposition (535 elements) of the semicircular enclosure.

modeling schemes becomes unobservable from the figure. Figs. 8(a) and (b) show the *p*-convergence characteristics of the DSEM for solving the dimensionless net radiative heat flux of the bottom wall with quadrilateral (uniform 25 elements, Q25) and triangular elements (T26), respectively, for single scattering albedo $\omega = 0$ and three different values of optical thickness, namely, $\tau_L = 0.1$, 1.0 and 10. The results obtained using the DSEM with 10th-order polynomial are considered as benchmark solution. Generally, the *p*-convergence rates are fast for both quadrilateral and triangular elements. In the case with large values of optical thickness, namely, $\tau_L = 10$, the *p*-convergence rates follow exponential law.

3.3. Case 3: radiative transfer problem with angular discontinuity induced by shielding of interior obstacle

We consider radiative transfer in non-scattering media in a semicircular enclosure with a circular hole as shown in Fig. 9. The media is kept hot (1000 K), while all other walls are black and kept cold (0 K). As shown in Fig. 10, we consider the angular distribution of radiative intensity of a node denoted *P* at the bottom wall. The incident radiative energy of node *P* comes from three regions, namely regions A–C. Because the interior circular obstacle shields radiative energy of region D from reaching node *P*, the incident radiative energy of node *P* coming from region B is weaker than that coming from region A and C. As a result, the angular distribution of radiative intensity of node *P* is remarkably non-uniform and contains discontinuity, thus the selected angular integration schemes should ensure that the radiative intensities coming from regions A–C

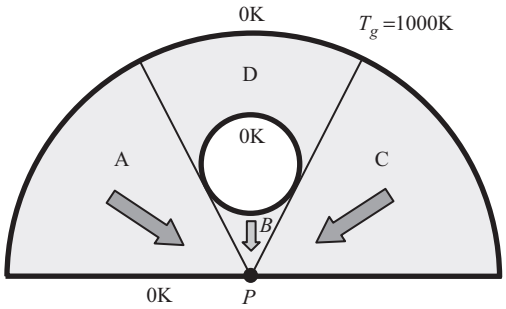

Fig. 10. Schematic diagram to illustrate the 'interior obstacle induced ray effect.'

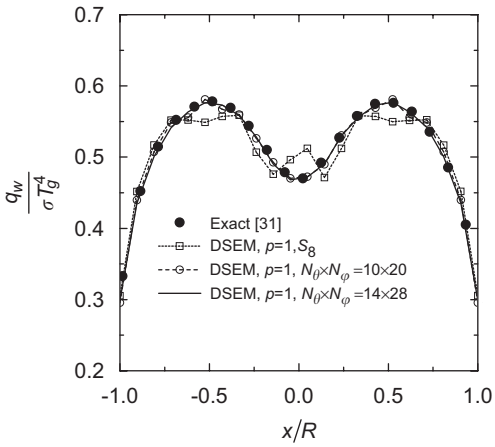

Fig. 11. Dimensionless net radiative heat flux distribution on the bottom wall of the semicircular enclosure for optical thickness $\tau_L = 1.0$.

being integrated accurately. Inaccuracy of the angular discretization scheme will cause 'wiggles' in the results of the RTE-based methods, which is also known as the 'ray effect' [27–29]. As this kind of ray effect is mainly caused by the shielding effect of the interior obstacle, here, we call this kind of ray effects as 'interior obstacle-induced ray effect', and another kind of ray effect will be discussed further in the next test case.

In the following analysis, The DSEM with local Lax-Friedrichs numerical flux scheme is applied to this case. The enclosure is decomposed into 535 triangular elements shown in Fig. 9. Fig. 11 shows the dimensionless net radiative heat flux distribution on the bottom wall for optical thickness $\tau_L = \beta R = 1.0$ obtained by the DSEM with first-order polynomial and three different angular discretization schemes, namely S_8 approximation, and PCA schemes [24,30] with $N_\theta \times N_\varphi = 10 \times 20$ and 14×28, and compared to the exact result of Kim et al. [31]. It can be seen that the 'wiggles' or ray effect of the solution obtained using S_8 approximation scheme is the strongest, which is attributed to its inaccuracy in integrating radiative intensity with remarkable non-uniformity. With the increasing of the accuracy of the angular discretization, the ray effect is effectively diminished. Generally, the DSEM is convergent, accurate and effective to solve the radiative transfer and can effectively bate this kind of ray effect.

Fig. 12(a)–(c) show comparison of the dimensionless net radiative heat flux distribution on the bottom wall obtained by the DSEM, the GSEM, and the LSSEM [23] under the same angular ($N_\theta \times N_\varphi = 14 \times 28$) and spatial discretization (535 triangular elements with first-order polynomial) for three different optical thicknesses, namely $\tau_L = \beta R = 0.1$, 1.0 and 10, respectively. The exact solution obtained by Kim et al. [31] is taken as benchmark. It can be seen that obvious wiggles exists in the results of the GSEM, which is attributed to the instability of continuous Galerkin formulation for solving convection-dominated problem. However, the results of the DSEM and the LSSEM are free of wiggles, and the DSEM give the best accuracy. The lack of accuracy of the LSSEM is attributed to large false scattering induced by discontinuity, while the DSEM

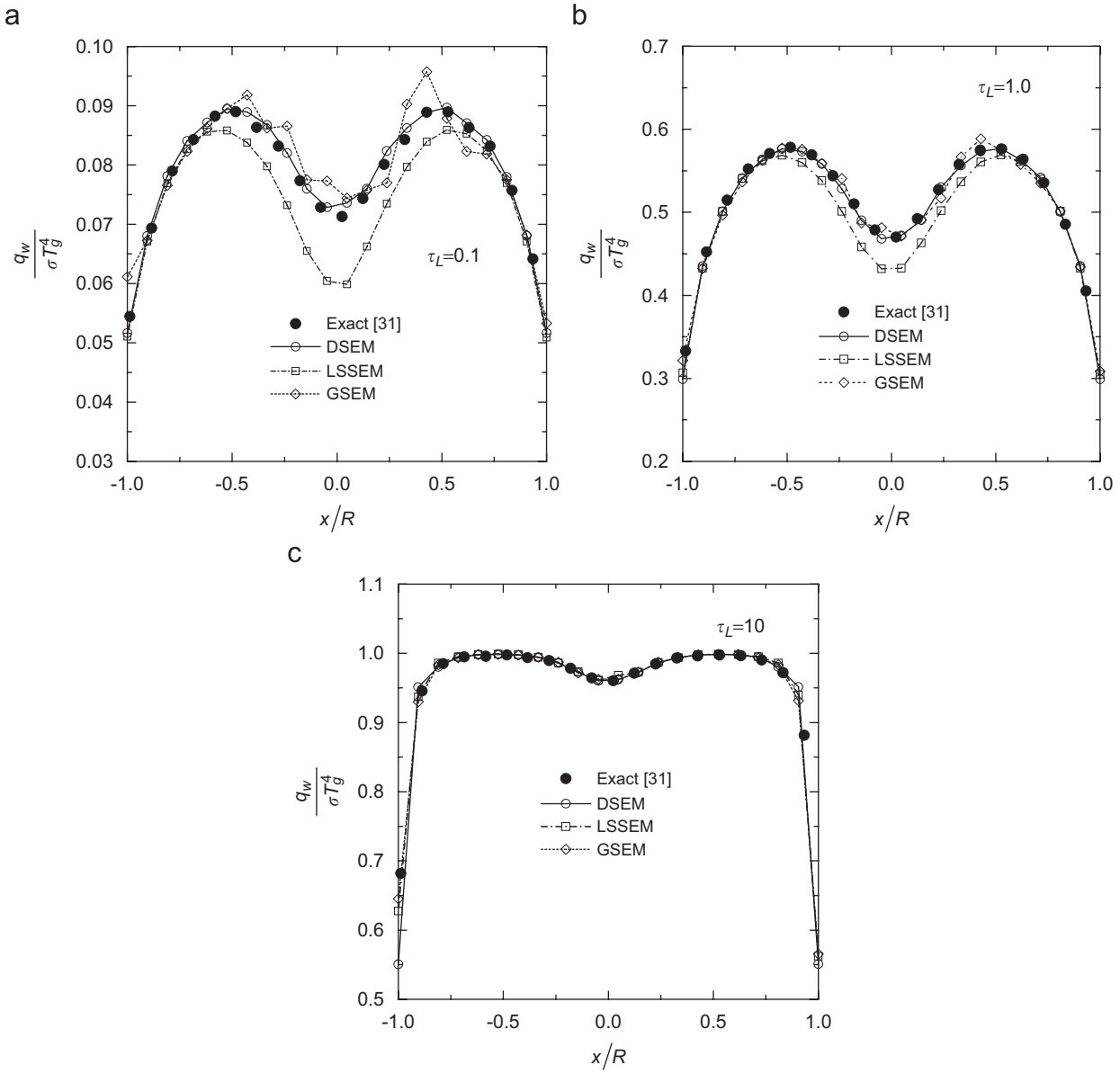

Fig. 12. Dimensionless net radiative heat flux distribution on the bottom wall of the semicircular enclosure for three values of optical thickness: (a) $\tau_L = 0.1$, (b) $\tau_L = 1.0$, and (c) $\tau_L = 10$.

brings less false scattering because the DG formulation brings minimal numerical diffusion. As compared to the GSEM and the LSSEM, the DSEM is accurate, stable and effective to solve radiative transfer in multidimensional semitransparent media with complex configuration.

3.4. Case 4: radiative transfer problem with angular discontinuity induced by boundary loading

In this case, the radiative transfer in a black square enclosure filled with isotropically scattering media with single scattering albedo $\omega = 1.0$ is considered. The optical thickness based on the side length L of the square is $\tau_L = 1.0$. The temperature of the bottom wall is kept $T_{w1} = 1000\,\mathrm{K}$, but all other walls and the media are kept cold (0 K). As shown in Fig. 13, the incident radiation energy of a node denoted P at the top wall comes from three regions, namely, regions A–C. Due to radiation from the high-temperature bottom wall, the radiative

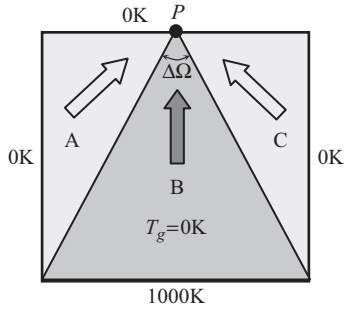

Fig. 13. Schematic diagram to illustrate the 'boundary induced ray effect.'

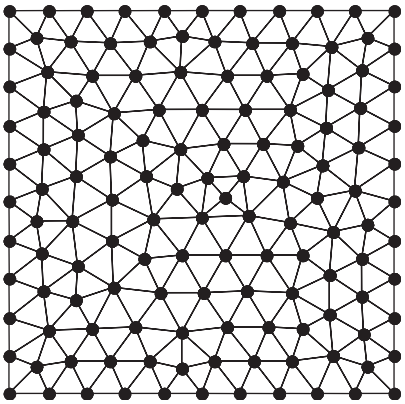

Fig. 14. Solution domain decomposition for the square enclosure (226 elements).

energy coming from region B is stronger than that coming from regions A and C. As a result, the angular integration accuracy of the radiative intensities of node P over 4π angular space is mainly attributed to the accuracy of integrating the radiative intensities coming from region B. Because the defined region B is different for different solution nodes on the top wall, thus it is difficult to do angular integration both efficiently and accurately. In this case, the ray effect is mainly caused by the non-uniform and discontinuity loading from the boundaries. Here, we call the ray effect of this kind as 'boundary induced ray effect'. It should be noted that two kinds of error existing in the numerical solution of the RTE, namely the 'ray effect' and the false scattering, and these errors interact with each other, such that the 'wiggles' in the solution may also be related to spatial discretization. In this case, for the node P at the top wall, the incident radiative intensity originated from the bottom wall is much less than that for the node P at other three walls. This means there is larger angular non-uniformity of radiative intensity at the top wall, thus it is very difficult to accurately integrate the angular distribution of radiative intensity. This case was studied by several researchers [28,32,33] and serves a good test case for test the performance of the numerical method.

The DSEM with local Lax-Friedrichs numerical flux scheme is applied to this case. The square enclosure is decomposed into 226 triangular elements as shown in Fig. 14. Here the PCA scheme [24,30] is used for angular discretization, in which the 4π angular space is decomposed into $N_\theta \times N_\varphi$ parts. Basically two spatial refinement strategies are available for the DSEM, namely, the h-refinement and p-refinement. First, the DSEM with first-order polynomial was applied to this case, and three different angular discretization schemes, namely, $N_\theta \times N_\varphi = 12 \times 24$, 16×32, and 20×40 are used. The dimensionless net radiative heat flux distributions on the top wall are shown in Fig. 15(a) and compared with the quasi-exact solution of Crosbie and Schrenker [32]. It can be seen that obvious 'wiggles' exist in the result of the DSEM when $N_\theta \times N_\varphi = 12 \times 24$, which is attributed to the less accuracy of angular discretization, while with the refining of the angular discretization, the 'wiggles' are effectively mitigated and smooth results are obtained.

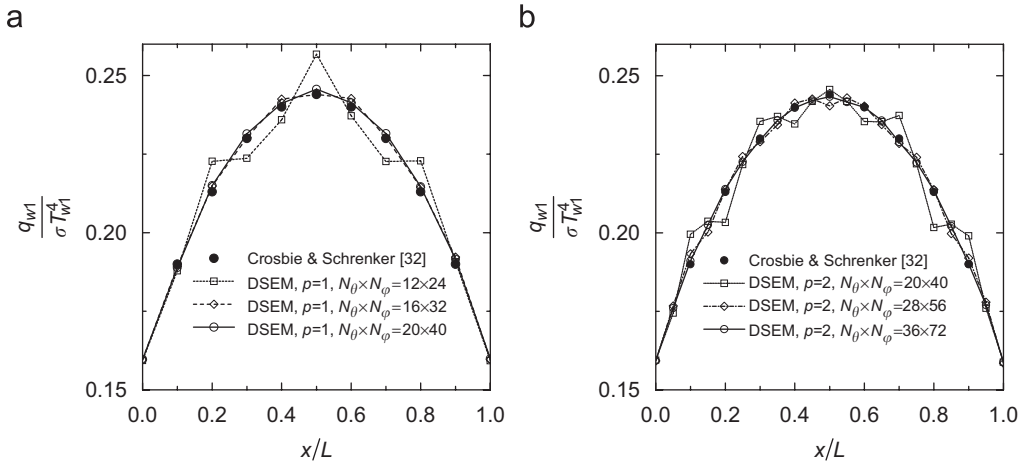

Fig. 15. Dimensionless net radiative heat flux distributions on the top wall of the square enclosure: (a) solution with first-order polynomial, (b) solution with second-order polynomial.

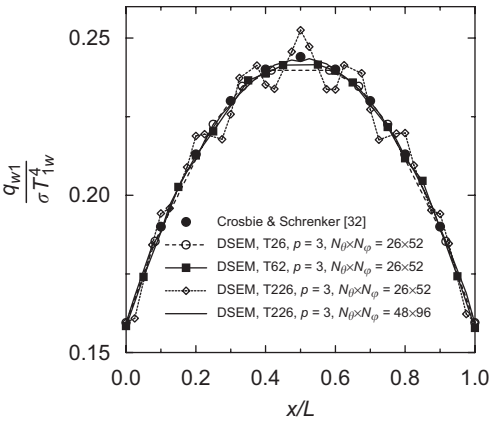

Fig. 16. Spatial *h*-refinement solution of the dimensionless net radiative heat flux distributions on the top wall.

To study the interaction of spatial discretization and angular discretization of the DSEM, we further consider applying the DSEM to this case with second-order polynomial. Fig. 15(b) shows the dimensionless net radiative heat flux distributions on the top wall for three angular discretization schemes, namely, $N_\theta \times N_\varphi = 20 \times 40$, 28×56, and 36×72. By comparison with Fig. 15(a), it can be seen that, in the case of $N_\theta \times N_\varphi = 20 \times 40$, the ray effect becomes stronger with increasing the polynomial order such that remarkable angular refinements are needed to mitigate the 'wiggles'. Then we consider the performance of the DSEM by just decreasing the element size, namely the performance of *h*-refinement. The DSEM is applied with third-order polynomial and the angular discretization is fixed to $N_\theta \times N_\varphi = 26 \times 52$. Fig. 16 shows the dimensionless net radiative heat flux distributions on the top wall for three spatial discretization schemes, namely, T26, T62 and T226. It can be seen that, even for the fixed angular discretization, the ray effect becomes stronger with decreasing the element size. However, when the angular discretization increases up to $N_\theta \times N_\varphi = 48 \times 96$, the 'wiggles' in the result obtained with spatial decomposition of T226 are effectively mitigated. It is well known that two kinds of error existing in the numerical solution of the RTE, namely the 'ray effect' and the false scattering. Like other methods, such as the DOM and the FVM, simultaneous refinements of both the spatial and the angular discretizations are needed for the DSEM to obtain accurate results. Because the DG formulation brings minimal numerical diffusion, the DSEM suffer little from false scattering, and the ray effect can be bated effectively from angular refinement. Generally, the DSEM is convergent, accurate and effective to solve the radiative transfer and can effectively bate the 'boundary-induced ray effect.'

4. Conclusions

A discontinuous spectral element method (DSEM) is presented to solve radiative heat transfer in multidimensional semitransparent media. This method is based on the general DG formulation, in which Chebyshev polynomial is used to build basis function on each element and both structured and unstructured elements are considered. The DSEM have properties such as *hp*-convergence, local conservation and solutions are allowed to be discontinuous across each element.

The DSEM with classical up-winding numerical flux scheme gives better results than the local Lax-Friedrichs numerical flux scheme on a coarse mesh while with mesh refining the difference between the results obtained through the two numerical flux modeling schemes becomes negligible. For the one-dimensional test case, the *p*-convergence rates of DSEM are very fast and follow exponential law for different values of extinction coefficient. For the two-dimensional test case, the *p*-convergence rates are fast for both quadrilateral and triangular elements, and follow exponential law for large optical thickness.

Two kinds of ray effect of the RTE-based numerical methods, namely the boundary-induced ray effect and the interior obstacle-induced ray effect, are studied. The DSEM brings less false scattering because the DG formulation brings minimal numerical diffusion, while the LSSEM suffers from large false scattering induced by discontinuity. Like other methods, such as the DOM and the FVM, simultaneous refinements of both the spatial and the angular discretizations are needed for the DSEM to obtain accurate results. The DSEM is convergent, accurate and effective to solve the radiative transfer problems in multidimensional semitransparent media with complex configuration and can effectively bate both the interior obstacle-induced ray effect and the boundary-induced ray effect.

Acknowledgments

The support of this work by the National Nature Science Foundation of China (50425619, 50336010) is gratefully acknowledged.

References

[1] Fiveland WA. Three-dimensional radiative heat-transfer solutions by the discrete-ordinates method. J Thermophys Heat Transfer 1988;2:309–16.
[2] Raithby GD, Chui EH. A finite-volume method for predicting a radiant heat transfer in enclosures with participating media. J Heat Transfer 1990;112:415–23.
[3] Chai JC, Lee HS. Finite-volume method for radiation heat transfer. J Thermophys Heat Transfer 1994;8:419–25.
[4] Murthy JY, Mathur SR. Finite volume method for radiative heat transfer using unstructured meshes. J Thermophys Heat Transfer 1998;12:313–21.
[5] Kisslelev VB, Roberti L, Perona G. An application of the finite-element method to the solution of the radiative transfer equation. JQSRT 1994;51:603–14.
[6] Liu LH. Finite element simulation of radiative heat transfer in absorbing and scattering media. J Thermophys Heat Transfer 2004;18:555–7.
[7] Howell JR, Perlmutter M. Monte Carlo solution of thermal transfer through radiant media between gray walls. J Heat Transfer 1964;86:116–22.
[8] Hottel HC, Cohen ES. Radiant heat exchange in a gas-filled enclosure allowance for nonuniformity of gas temperature. AIChE J 1958;4:3–14.
[9] Cui X, Li BQ. Discontinuous finite element solution of 2-D radiative transfer with and without axisymmetry. JQSRT 2005;96:383–407.
[10] Cui X, Li BQ. A discontinuous finite-element formulation for internal radiation problems. Numer Heat Transfer B 2004;46:223–42.
[11] Liu LH, Liu LJ. Discontinuous finite element method for radiative heat transfer in semitransparent graded index medium. JQSRT 2007;105:377–87.
[12] Bassi F, Rebay S. High-order accurate discontinuous finite element solution of the 2D Euler equations. J Comput Phys 1997;138:251–85.
[13] Cockburn B, Shu CW. The Runge–Kutta discontinuous Galerkin method for conservation laws v: multidimensional systems. J Comput Phys 1998;141:199–224.
[14] Baumann CE, Oden JT. A discontinuous *hp* finite element method for convection–diffusion problems. Comput Methods Appl Mech Eng 1999;175:311–41.

[15] Warburton TC, Karniadakis GE. A discontinuous Galerkin method for the viscous MHD equations. J Comput Phys 1999;152:608–41.
[16] Cockburn B. Discontinuous Galerkin methods. ZAMM 2003;83:731–54.
[17] Cockburn B, Karniadakis GE, Shu CW. The development of discontinuous Galerkin methods. In: Cockburn B, Karniadakis GE, Shu CW, editors. Discontinuous Galerkin methods: theory, computation and applications. Berlin: Springer; 2000. p. 3–50.
[18] Patera AT. A spectral element method for fluid dynamics–laminar flow in a channel expansion. J Comput Phys 1984;54:468–88.
[19] Henderson RD, Karniadakis GE. Unstructured spectral element methods for simulation of turbulent flows. J Comput Phys 1995;122:191–217.
[20] Karniadakis GE, Sherwin SJ. Spectral/*hp* element methods for CFD. New York: Oxford University Press; 1999.
[21] Deville MO, Fischer PF, Mund EH. High-order methods for incompressible fluid flow. Cambridge: Cambridge University Press; 2002.
[22] Chai JC, Lee HS, Patankar SV. Finite-volume method for radiation heat transfer. In: Minkowycz WJ, Sparrow EM, editors. Advances in numerical heat transfer, vol. 2. New York: Taylor & Francis; 2000. p. 109–41.
[23] Zhao JM, Liu LH. Least-squares spectral element method for radiative heat transfer in semitransparent media. Numer Heat Transfer B 2006;50:473–89.
[24] Zhao JM, Liu LH. Solution of radiative heat transfer in graded index media by least square spectral element method. Int J Heat Mass Transfer (2007), doi:10.1016/j.ijheatmasstransfer.2006.11.032.
[25] Zhao JM, Liu LH. Second order radiative transfer equation and its properties of numerical solution using finite element method. Numer Heat Transfer B 2007;51:391–409.
[26] Kim TK, Lee H. Effect of anisotropic scattering on radiative heat transfer in two-dimensional rectangular enclosures. Int J Heat Mass Transfer 1988;31:1711–21.
[27] Chai JC, Lee HS, Patankar SV. Ray effect and false scattering in the discrete ordinates method. Numer Heat Transfer B 1993;24:373–89.
[28] Ramankutty MA, Crosbie AL. Modified discrete ordinates solution of radiative transfer in two-dimensional rectangular enclosures. JQSRT 1997;57:107–40.
[29] Coelho PJ. A modified version of the discrete ordinates method for radiative heat transfer modelling. Comput Mech 2004;33:375–88.
[30] Liu LH, Zhang L, Tan HP. Finite element method for radiation heat transfer in multi-dimensional graded index medium. JQSRT 2006;97:436–45.
[31] Kim MY, Baek SW, Park JH. Unstructured finite-volume method for radiative heat transfer in a complex two-dimensional geometry with obstacles. Numer Heat Transfer B 2001;39:617–35.
[32] Crosbie AL, Schrenker RG. Radiative transfer in a two-dimensional rectangular medium exposed to diffuse radiation. JQSRT 1984;31:339–72.
[33] Larsen ME, Howell JR. The exchange factor method: an alternative zonal formulation of radiating enclosure analysis. J Heat Transfer 1985;107:936–42.